

Contents lists available at ScienceDirect

Surface Science

journal homepage: www.elsevier.com/locate/susc





Synthesis of Pd@Rh nanocubes with well-defined {100} surface and controlled shell thicknesses for the fabrication of Rh nanocages

Chenxiao Wang ^{a,1}, Ying Lyu ^{b,1}, Younan Xia ^{a,b,*}

- a School of Chemistry and Biochemistry. Georgia Institute of Technology. Atlanta. GA 30332, United States
- b The Wallace H. Coulter Department of Biomedical Engineering, Georgia Institute of Technology and Emory University, Atlanta, GA 30332, United States

ARTICLE INFO

Keywords: Rhodium Core-shell nanocrystals Facet control Thermal stability Nanocages

ABSTRACT

We report a facile synthesis of Pd@Rh core-shell nanocubes with ultrathin Rh shell and well-defined, smooth {100} facets for the production of Rh cubic nanocages. Under carefully optimized conditions, the deposition and diffusion rates of Rh adatoms on Pd cubic seeds can be tuned to a suitable level to enable the layer-by-layer growth of Rh overlayers. Specifically, the reaction temperature, type of Rh precursor, injection rate of the precursor solution, in addition to the size of the Pd seeds, all play an important role in establishing the desired growth mode while preventing island growth and homogeneous nucleation. The Rh shell not only endows the nanocrystals with significantly enhanced shape stability against thermally activated transformation under heating up to 500 °C, but also enables the production of Rh nanocages with ultrathin walls and well-preserved {100} facets, which to our knowledge has not been reported in literature.

1. Introduction

Nanocrystals based on Rh have received great interests as heterogeneous catalysts with superior performance in a wide variety of reactions, including CO oxidation [1], NO reduction [2], and hydrogenations [3]. They have found commercial use as one of the key components in the three-way catalytic converters for automobiles [4]. However, as one of the rarest elements in the Earth's crust [5], the scarcity and thus high price of Rh have hindered its large-scale applications. As such, there is an urgent need to increase the utilization efficiency of Rh atoms. To this end, Rh nanocrystals with controlled shapes and twin structures, including cubes [6,7], octahedra [7], decahedra [8], icosahedra [9], hexagonal plates [10], and concave cubes [11], have been synthesized and tested as heterogeneous catalysts in an effort to enhance the specific activity by optimizing their surface structures. As an alternative to this strategy, core-shell structures, with Rh as the shell and another metal as the core, have been synthesized with different shapes to help increase the surface exposure of Rh atoms [12]. The interior atoms in these structures, however, are still blocked from interacting with reactant molecules. As a solution to this issue, hollow nanostructures such as nanoframes have been fabricated, but this type of nanostructures fail to control the type of facet exposed on the surface

[11].

In recent years, nanocages have emerged as a new type of hollow nanostructure featuring both high surface exposure and well-defined surface structure [13]. With sub-nanometer thin walls and capped by a certain type of facets (usually {100} or {111}), they have emerged as promising candidates for catalytic applications with both high activity and selectivity. Notable examples include Pt-based octahedral nanocages toward oxygen reduction [14], Ir-based cubic nanocages toward water oxidation [15], and Ru-based icosahedral nanocages for hydrazine decomposition [16]. The nanocages were prepared by depositing a thin layer of the desired metal onto Pd nanocrystals (i.e., seeds or templates) of different shapes, followed by removal of the Pd core through selective etching to leave behind the nanocages. Despite successful synthesis of several types of nanocages of platinum-group metals (PGMs), it remains a challenge to produce Rh-based nanocages through the same approach. In a previous study, we demonstrated the synthesis of Pd@Rh nanocrystals by depositing Rh on Pd nanocrystals of 6-7 nm in size using Rh(OAc)₃ as the precursor [12]. Due to the fast reduction kinetics of this precursor, the reaction temperature was restricted to 185 °C to avoid homogeneous nucleation, which limited the surface diffusion of Rh adatoms on the surface of the seeds. This was especially problematic in the case of nanocubes where the lower coordination of atoms

E-mail address: younan.xia@bme.gatech.edu (Y. Xia).

^{*} Corresponding author.

¹ These authors contributed equally to this work.

on the {100} surface of cubic seeds (as compared with the {111} surface of octahedral seeds) carries a higher energy barrier to surface diffusion [17]. As a result, layer-by-layer growth mode were only partially achieved when seeds of very small sizes (6–7 nm) were involved and the synthesis failed when switching to seeds of larger sizes (i.e., 18 and 37 nm in that study). Moreover, when examined under high-resolution transmission electron microscope (HRTEM), concavities, terraces, and steps were observed on the side faces due to inadequate surface diffusion. When these particles are subject to oxidative etching, the three-dimensional structure of the nanocages tend to collapse due to their uneven shell thickness and thus weak mechanical strength.

Herein we report a synthetic protocol to synthesize Pd@Rh nanocrystals featuring smooth, well-defined {100} facets and larger size for the successful preparation of Rh nanocages. Sodium hexachlororhodate (III) (Na₃RhCl₆) with lower reactivity than Rh(OAc)₃ (0.431 V_{SHE} for $RhCl_6^{3-} + 3e \rightarrow Rh + 6Cl_7$, as compared with 0.758 V_{SHE} for $Rh^{3+} + 3e \rightarrow$ Rh) [18] was used as a precursor to reduce the reaction rate and thus avoid homogeneous nucleation. The Br ions from KBr serve as a bifunctional ligand to further slowdown the reaction through ligand exchange [19] and promote the formation of Rh(100) surface [6]. The reaction was conducted at a high temperature of 210 °C to promote surface diffusion. Benefiting from the complete coverage of atomically thin Rh overlayer, the core-shell nanocubes exhibited significantly improved thermal stability when benchmarked against Pd monometallic counterparts through in situ electron microscopy observation. Through chemical wet etching of the core-shell nanocubes, Rh nanocages with well-defined {100} surface and ultrathin walls were successfully fabricated.

2. Experimental section

2.1. Chemicals and materials

Triethylene glycol (TEG, 99%) was purchased from J. T. Baker. Poly (vinyl pyrrolidone) (PVP, with an average molecular weight of 55,000), potassium chloride (KCl, 99%), potassium bromide (KBr, 99%), hydrochloric acid (HCl, 37%), iron(III) chloride (FeCl₃, 97%), sodium hexachlororhodate(III) (Na₃RhCl₆, 97%), rhodium(III) acetylacetonate (Rh (acac)₃, 97%) were obtained from Sigma-Aldrich. L-ascorbic acid (AA, 99%) was ordered from BioXtra. Ethanol (anhydrous) was ordered from KOPTEC. Acetone was obtained from VWR Chemicals BDH. Syringes and syringe pump were purchased from KD Scientific. The temperatures of all syntheses were monitored using a thermal sensor acquired from ACE Glass. Aqueous solutions were prepared using deionized (DI) water with a resistivity of 18.2 M Ω -cm at room temperature.

2.2. Synthesis of Pd cubes with different sizes

Pd cubes were synthesized according to a protocol reported by our group. In a typical synthesis of 18-nm Pd cubes, 8.0 mL of an aqueous solution containing PVP (105 mg), AA (60 mg), and KBr (600 mg) was placed in a 20-mL vial and pre-heated at 80 $\,^{\circ}\mathrm{C}$ for 10 min under magnetic stirring (400 rpm). Afterwards, 3.0 mL of an aqueous solution containing 57 mg of Na₂PdCl₄ was added using a pipette. After the vial had been capped, the reaction was continued at 80 $\,^{\circ}\mathrm{C}$ for 3 h. The solid products were collected by centrifugation and washed three times with water, and then re-dispersed in water for further use. For the synthesis of 6-nm cubes, 5 mg KBr and 185 mg KCl were added instead.

2.3. Synthesis of Pd@Rh nanocubes with different sizes and shell thicknesses

In a typical synthesis of 18-nm Pd@Rh $_{3L}$ nanocubes, 5 mL of a TEG solution containing Pd cubes (0.48 mg), AA (25 mg), KBr (50 mg), and PVP (100 mg) was transferred into a glass vial and heated at 210 $\,^{\circ}$ C under magnetic stirring (380 rpm) for 10 min. After that, 5 mL of

another TEG solution containing 0.63 mg of Na_3RhCl_6 and 100 mg PVP was added into the flask at 0.25 mL h^{-1} . After all the precursor solution had been added, the reaction was continued for another one hour and solid products were then collected by precipitation with acetone, washed three times with a mixture of ethanol and acetone, and finally re-dispersed in water for further use. To obtain Pd@Rh_{1.5} L and Pd@Rh_{0.6} L, the amounts of precursor solution added were reduced to 3 mL and 1 mL, respectively. To obtain 8-nm Pd@Rh nanocubes, 0.18 mg of the 6-nm Pd cubes were used instead.

2.4. Formation of Rh nanocages

Chemical etching was conducted in an acidic aqueous solution to generate Rh nanocages. Typically, 1 mL of the as-prepared Pd@Rh nanocubes was dispersed in a mixture containing 50 mg of KBr, 50 mg of PVP, 10 mg of FeCl₃, 0.06 mL of Hcl (37%), and 6 mL of H₂O and then heated at 80 °C under magnetic stirring (380 rpm) for 1 h. Afterwards, the solid product was collected by centrifugation, washed three times with ethanol, and finally re-dispersed in water for further characterization.

2.5. Characterizations

Transmission electron microscopy (TEM) images were taken using a Hitachi HT7700 microscope operated at 120 kV. High-angle annular dark-field scanning transmission electron microscopy (HAADF-STEM) images and energy-dispersive X-ray (EDX) spectroscopy mapping data were acquired on an aberration-corrected Hitachi HD-2700 STEM operated at 200 kV. Inductively coupled plasma mass spectrometry (ICP-MS, NexION 300Q, PerkinElmer) was used to determine the metal contents in the as-obtained nanocrystals. X-ray diffraction (XRD) patterns were obtained with a PANalytical X'Pert PRO Alpha-1 diffractometer using a 1.8 kW ceramic copper tube source. The X-ray photoelectron spectroscopy (XPS) data were collected on a Thermo K-Alpha spectrometer with an Al K α source.

3. Results and discussion

We first synthesized Pd nanocubes with an average edge length of 16.2 nm (Figure S1) according to a protocol developed by our group [20]. After that, we deposited Rh shells on the Pd nanocubes in a layer-by-layer manner by dropwise adding a TEG solution containing Na₃RhCl₆ and PVP into another solution containing TEG, PVP, KBr, and AA under magnetic stirring over a course of 20 h. In this synthesis, AA acted as a reducing agent; TEG served as both a solvent and a precursor to a co-reducing agent; PVP was a colloidal stabilizer. On the other hand, KBr was an additive that had a multifaceted impact on the outcome of the synthesis, which will be discussed later in detail. The synthesis was conducted at a temperature of 210 °C to promote the diffusion of Rh adatoms on Pd surface. Fig. 1A shows a typical TEM image of the as-obtained Pd@Rh core-shell nanocubes, confirming a uniform size and shape of the sample. Unlike previously reported products that were plagued by island growth of Rh and a second population of Rh particles arising from homogeneous nucleation [12], the current product shows 100% layer-by-layer growth for the Rh atoms. The atomic composition of the product was determined to be Pd_{81.6}Rh_{18.4} using ICP-MS, which corresponds to ca. three atomic overlayers of Rh on the Pd surface based on an inter-planar distance of 0.19 nm for the {200} planes of face-centered cubic (fcc) Rh and the 16.2-nm size of the Pd nanocubes. It is worth mentioning that similar product could be obtained when the Na₃RhCl₆ precursor is replaced with the same amount of Rh(acac)₃ (Figure S2), because Rh(acac)3 is known to have moderate reduction kinetics even at elevated temperatures [7].

Fig. 1B–E shows high-angle annular dark-field scanning TEM (HAADF-STEM) images taken from a number of adjacent core–shell nanocubes, demonstrating smooth side faces and sharp corners for each

C. Wang et al. Surface Science 736 (2023) 122339

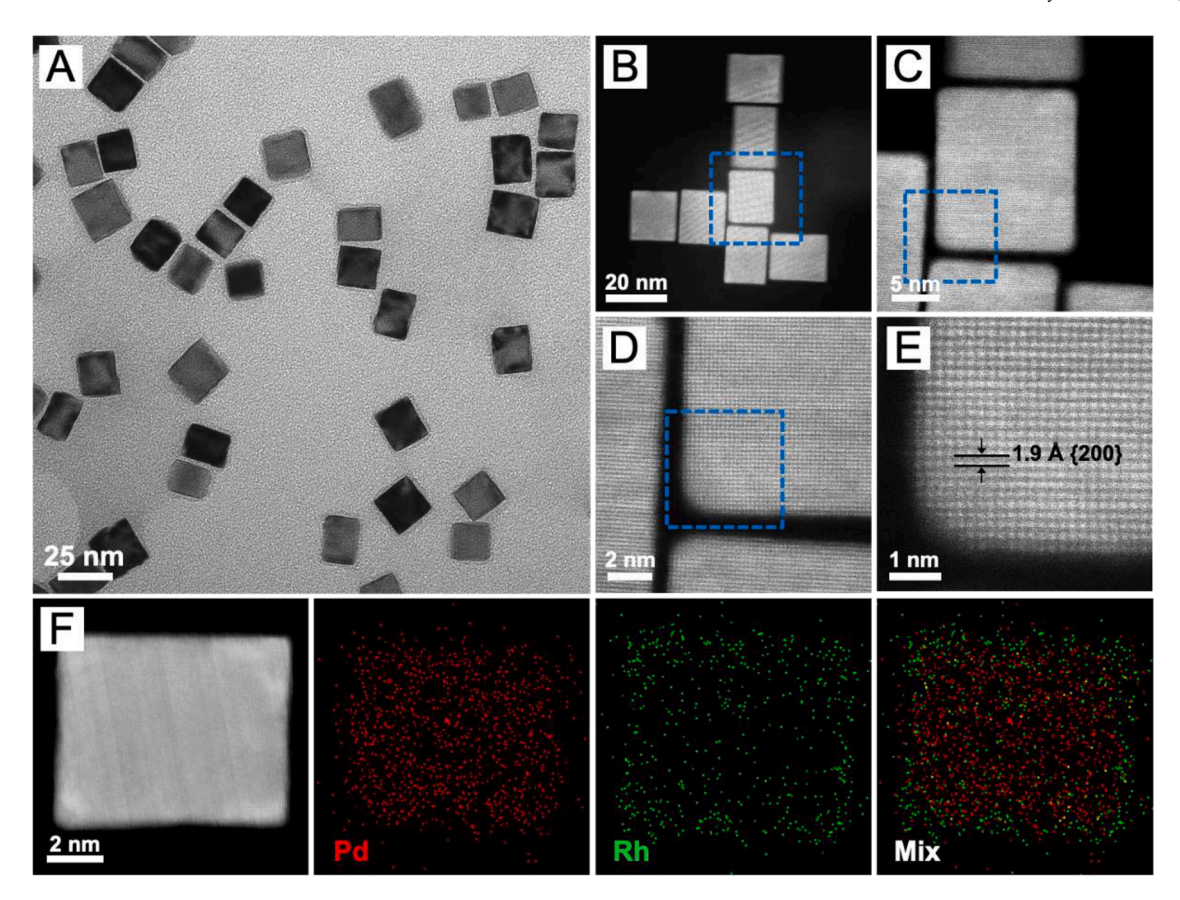


Fig. 1. (A) A typical TEM image of the $Pd@Rh_{3L}$ nanocubes. (B–E) HAADF-STEM images of the $Pd@Rh_{3L}$ nanocubes at different magnifications. (F) HAADF-STEM image of an individual $Pd@Rh_{3L}$ nanocube and the corresponding EDX mappings of Pd and Rh elements.

nanocube. No atomic terraces, steps, or concavity was observed in the atomic-resolution image shown in Fig. 1E. Fig. 1F shows EDX mapping of an individual Pd@Rh nanocube, revealing the core—shell spatial distribution of the two elements. The chemical states of the two metals were further analyzed by XPS. As shown in Figure S3, the characteristic doublets of 3d orbitals of Rh and Pd were clearly resolved. Each elemental peak was dominated by the zero-valent state, with a very small portion for the oxidated species.

In order to verify the layer-by-layer growth mode during this synthesis, we reduced the volume of Rh precursor solution added from 5 mL to 3 and 1 mL, respectively. From the TEM images and corresponding HAADF-STEM images of the two samples shown in Fig. 2, they exhibit a morphology similar to that of the Pd@Rh $_{\rm 3L}$ sample, including smooth side faces down to atomic scale. No self-nucleated particles were observed, eliminating the possible involvement of Ostwald ripening in the deposition of Rh onto the surface of Pd seeds. The atomic

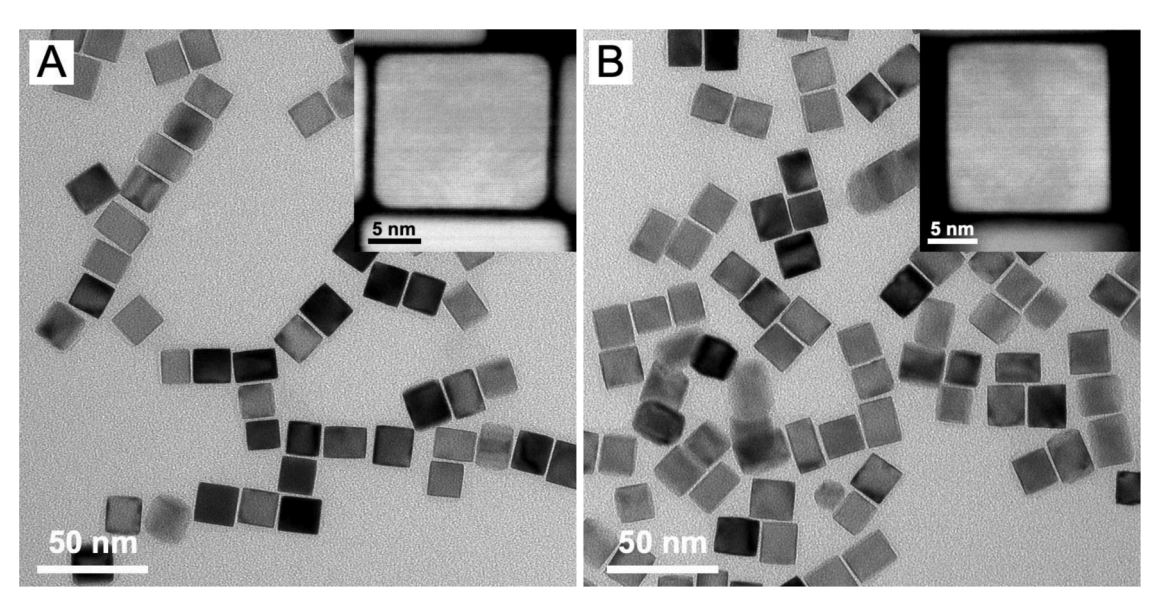


Fig. 2. (A) TEM and HAADF-STEM (inset) images of the Pd@Rh₀,6L nanocubes. (B) TEM and HAADF-STEM (inset) images of Pd@Rh₁,5L nanocubes.

compositions (summarized in Table 1) of these two products were determined to be $Pd_{96.0}Rh_{4.0}$ and $Pd_{89.7}Rh_{10.3}$, respectively, which corresponds to 0.6 and 1.5 atomic layers of Rh. In other words, the Rh atoms were indeed deposited on the seeds in a layer-by-layer fashion, with every 1 mL of the precursor solution contributing to $\it ca.$ 0.5 layers of the Rh shell. Note that the atomic percentages of Rh in these samples were lower than the ideal values calculated from the amounts of Pd cubes and Rh precursor added. Specifically, the ideal atomic percentages of Rh were supposed to be 10.9, 19.5, and 26.6% after the addition of 1, 3, and 5 mL of Rh precursor solutions, respectively. The loss of Rh mass during the synthesis can be attributed to the incomplete reduction of the precursor and the formation of Rh clusters that were too small to be collected through centrifugation.

Next, we analyzed the surface compositions of the core–shell nanocubes with different shell thicknesses through cyclic voltammetry (CV) scanning in an aqueous electrolyte containing 0.1 M HClO₄ (Fig. 3). It has been established that the Pd (100) surface shows characteristic voltametric peaks in the hydrogen underpotential deposition region between 0.2–0.3 $V_{\rm RHE}$ but there is no such peak for Rh(100) [7,21]. Indeed, two distinct peaks could be observed in the CV curve of pristine Pd nanocubes (Fig. 3A). As more Rh was deposited onto the Pd{100} facets to form 0.6, 1.5, and finally 3 atomic layers of Rh (Fig. 3B–D), the relative intensities of the voltametric peaks of Pd gradually decreased and eventually became negligible. These results indicated that the surface of the Pd@Rh_{3L} nanocubes was dominated by Rh instead of Pd–Rh alloy, which can be attributed to the immiscibility and thus spontaneous phase segregation between Rh and Pd over the entire composition range [22].

It is worth emphasizing that a careful control over the reaction conditions, including the injection rate and amount of precursor solution, the reaction temperature, and the additives, is essential to the formation of a smooth surface. During the synthesis, the injection rate of the precursor had to be controlled at a low level in order to keep the concentration of Rh atoms in the reaction mixture at a low level to avoid supersaturation and homogeneous nucleation. In the standard protocol, the injection rate was carefully controlled at 0.25 mL h⁻¹ using a syringe pump. As a comparison, when this rate was increased to 0.5 mL h⁻¹, a second population of particles (arising from homogeneous nucleation) with sizes significantly smaller than the Pd cubic seeds became visible in the TEM image (Figure S4A). As discussed in Fig. 2, the amount of precursor injected is also important as it directly controls the thickness of the Rh shell. Unfortunately, the Rh shell could not grow thicker than three atomic layers without altering the growth mode. As shown in Figure S4B, when 7.8 mL of precursor solution was added, island growth was triggered on top of the smooth Rh shell due to inadequate surface diffusion, generating spikes from the corners of each nanocube. Interestingly, each spike showed a rectangular shape with right angles under TEM, indicating a {100}-terminated surface. This could be attributed to the {100}-selective capping effect from Br ions [6,23]. Moreover, the complex roles of KBr additive should not be overlooked. It has been established that Br could bind to Rh(III) ions to form a stable complex with lower reactivity, thus changing the reaction rate constant of the precursor and slowing down the redox reaction [19]. Indeed, without the addition of KBr, the fast reduction of the Rh precursor would result in homogeneous nucleation and formation of tiny Rh particles instead of Rh shell (Figure S4C). Taken together, all the reaction parameters must

Table 1Compositions of Pd@Rh nanocubes with different shell thicknesses determined using ICP-MS.

Sample	Atomic Percentage (%)	
	Pd	Rh
Pd@Rh _{0.6L}	96.0	4.0
Pd@Rh _{1.5L}	89.7	10.3
Pd@Rh _{3L}	81.6	18.4

be optimized in order to generate Pd@Rh nanocubes with a smooth surface while eliminating impurities such as surface islands and small Rh particles.

Similar to the injection rate, reaction temperature is another essential parameter that must be carefully controlled because it influences both the reduction rate of the Rh precursors (i.e., the deposition rate of the Rh atoms) and the surface diffusion rate of Rh adatoms. If the temperature was reduced to 190 °C (Figure S5A), the Rh metal mainly existed as self-nucleated small particles instead of a shell on the surface of Pd cubes. This could be attributed to the stronger binding of Br to the Pd(100) surface at a relatively low temperature. The surface-adsorbed Br would block the access of Rh atoms to the Pd surface and force them to self-nucleate and generate individual particles [24]. On the other hand, when subject to a higher temperature of 230 °C (Figure S5B), the faster reduction of the precursor and thus a higher rate of atom supply led to a deposition rate greater than surface diffusion, triggering island growth that made the surface rough and irregular.

As a catalytic metal, Rh is widely used to promote heterogeneous thermal catalytic reactions, such as syngas production and vehicle exhaust treatment, that are operated at elevated temperatures. In order to study the thermal stability of Pd@Rh nanocubes for potential application as thermal catalysts, we loaded the Pd and Pd@Rh samples onto a chip with 30-50 nm-thick SiN_x membrane surrounded by a heating circuit and subjected them to in situ heating and observation in TEM. As shown in Fig. 4, the original shapes of both samples exhibited sharp corners and smooth edges at room temperature. However, as the temperature was elevated, the shape evolution of these two samples started to differ. After being heated at 300 °C in vacuum for 30 min, the corners of each Pd cube became truncated and those close to each other started to merge together. For Pd@Rh cubes, in contrast, essentially no shape change was observed. When the temperature was further increased to 400 $\,^{\circ}\text{C}$ and then 500 $\,^{\circ}\text{C}$, individual Pd cubes became more rounded and the particles in touch started to fuse into one particle with uniform contrast under TEM. On the contrary, the cubic shape of the Pd@Rh nanocubes was still well preserved, with only slight corner truncation. At a high temperature of 600 °C, the Pd nanocubes became nearspherical while the Pd@Rh nanocubes possessed a morphology similar to that of the Pd sample at 300 °C. Taken together, with the full coverage by and protection from refractory Rh overlayer on Pd surface, the Pd@Rh nanocubes exhibited a thermal stability almost 300 °C higher than pristine Pd nanocubes of similar sizes, making the former promising candidate as thermal catalysts with higher utilization efficiency than pure Rh nanocrystals and uncompromised great thermal stability.

As noted earlier, the well-defined core-shell structure with smooth, three atomic layer-thick Rh shell could benefit the production of Rh nanocages by removing Pd in the core to leave behind Rh shell only. Owing to the relatively large difference in redox potential between $\mathrm{Fe^{3+}/Fe^{2+}}$ and $\mathrm{PdBr_4^{2-}/Pd}$ (0.77 $\mathrm{V_{SHE}}$ for $\mathrm{Fe^{3+}/Fe^{2+}}$ vs. 0.49 $\mathrm{V_{SHE}}$ for PdBr₄²/Pd) [11], this process can be easily achieved by treating the core-shell particles in an aqueous etchant containing KBr, FeCl₃, and HCl at 80 °C for 1 h. In the etching process, the Fe³⁺ from FeCl₃ served as an oxidizing agent to react with the Pd atoms in the core whereas Br coordinated with the resultant Pd²⁺ to form PdBr₄²⁻ which was then dissolved into the aqueous solution and removed from the nanocrystals. The use of HCl helped prevent both Fe³⁺ and Fe²⁺from hydrolysis. Fig. 5A and B shows typical TEM and HAADF-STEM images of the as-obtained Rh nanocages, respectively. A lattice spacing of 1.9 Å could be measured from the atomic-resolution image in Fig. 5C, in agreement with the value obtained in Fig. 1E. This result demonstrated that the crystal structure of the Rh shell was well-preserved during the etching process. We conducted ICP-MS to quantitatively analyze the elemental composition of the product. The atomic percentage of Rh increased from 18.4% to over 90% after the etching of Pd core, indicating a highly efficient and selective Pd removal process. Taken together, these data confirmed that the nanocages were essentially made of Rh. In order to

C. Wang et al. Surface Science 736 (2023) 122339

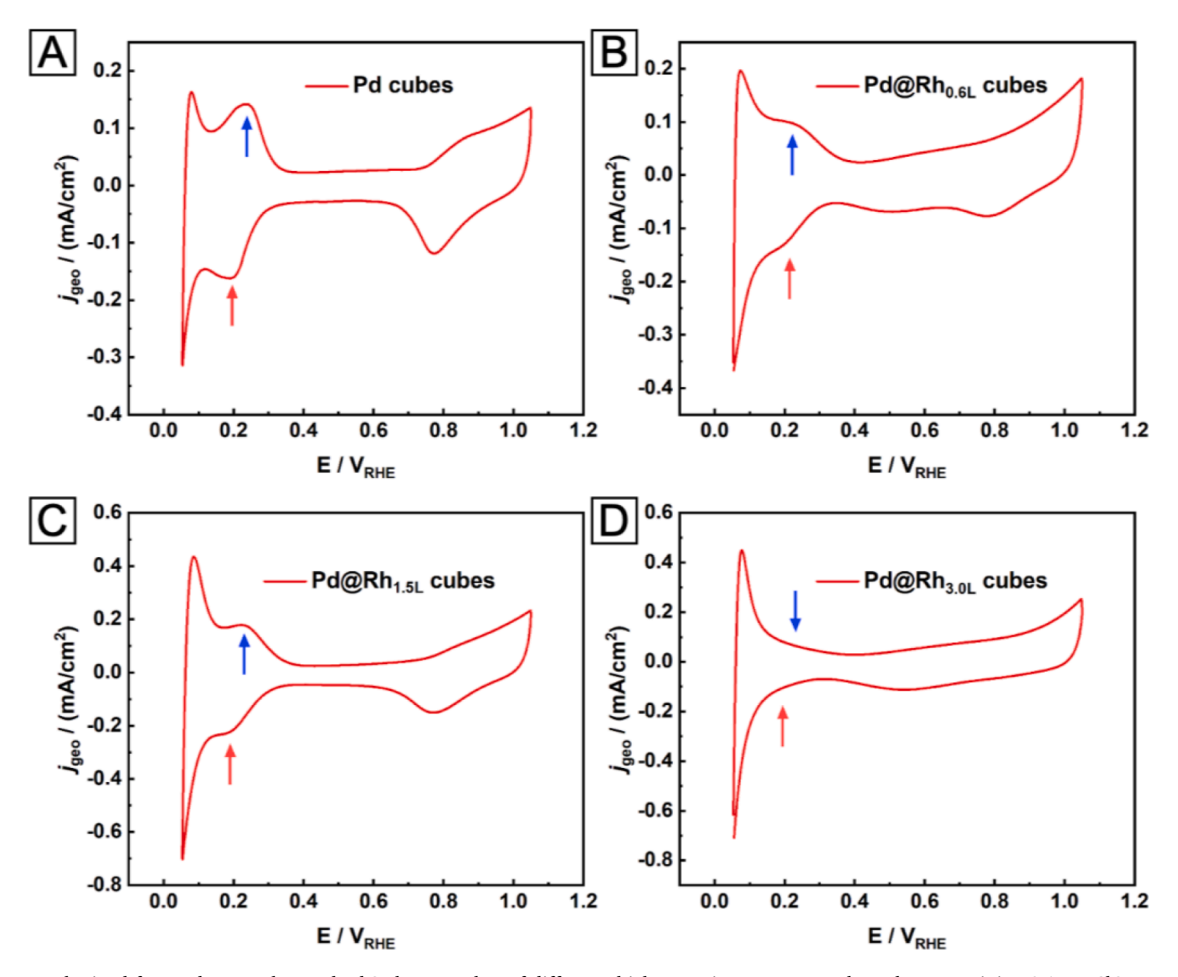


Fig. 3. CV curves obtained from Pd nanocubes and Pd@Rh nanocubes of different thicknesses in an aqueous electrolyte containing $0.1M\ HClO_4$.

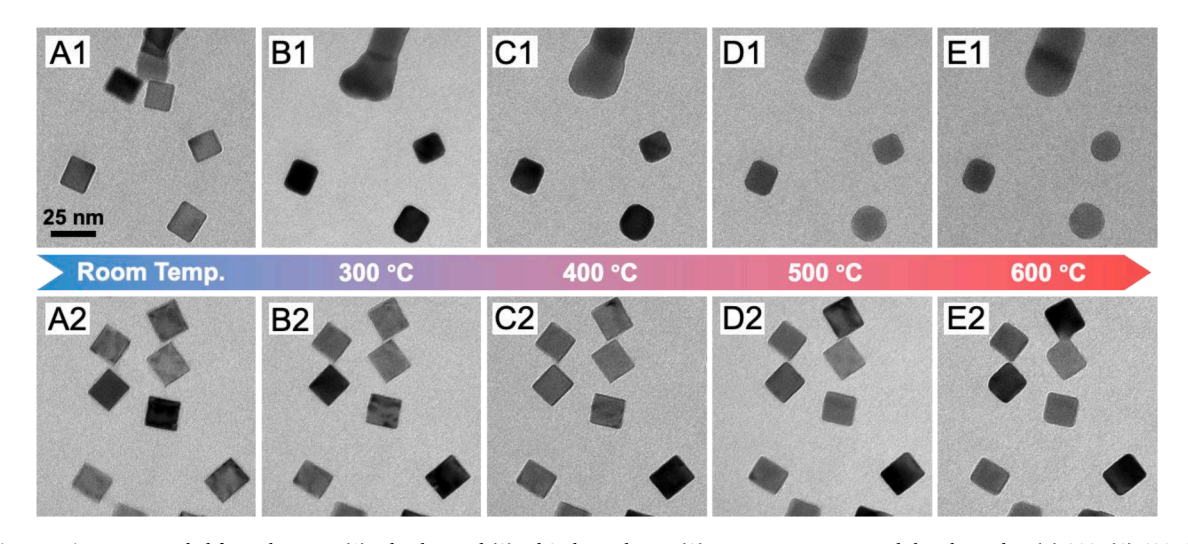


Fig. 4. In situ TEM images recorded from the same (1) Pd cubes and (2) Pd@Rh $_{3L}$ cubes at (A) room temperature and then heated to (B) 300, (C) 400, (D) 500, and (E) 600 $\,^{\circ}$ C for 30 min, respectively. The scale bar in (A1) applies to all panels.

demonstrate the necessity of using Pd nanocubes of larger sizes as seeds, Pd@Rh nanocrystals of smaller sizes were also prepared by employing Pd cubes of smaller sizes as seeds for the production of Rh nanocages as a comparison (Figure S6). It is obvious from the TEM images that core—shell nanocrystals possess different types of structural defects, including corner truncations, terraces, and steps (Figure S6A). The nanocages produced from these products are comprised of incomplete structure

and debris (Figure S6B).

4. Conclusion

In summary, we have demonstrated the synthesis of Pd@Rh coreshell nanocubes with an ultrathin Rh shell and well-defined {100} facets. Under optimized injection rate of the precursor and reaction

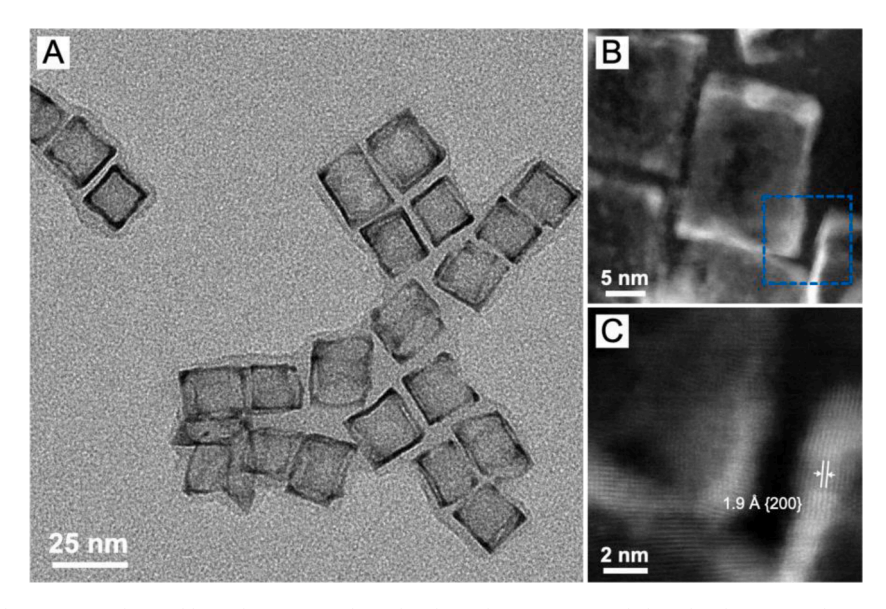


Fig. 5. (A) A TEM image of Rh nanocages obtained by etching away Pd in Pd@Rh_{3L} cubes using an FeCl₃-based etchant. (B and C) HAADF-STEM images of Rh cages at two different magnifications.

temperature, together with the addition of KBr, the growth mode was adjusted to layer-by-layer instead of surface island growth or self-nucleation. The complete coating of Pd nanocubes by a Rh shell significantly enhanced their thermal stability, as established by *in situ* TEM observation. Moreover, Rh nanocages with ultrathin walls could be readily fabricated through wet etching. We also found that the size of the Pd seeds is of critical importance for generating a uniform shell with high mechanical strength to keep the nanocages from collapse during the etching process. It is expected that the method reported here will facilitate the development of novel catalysts with high utilization efficiency of precious metals in addition to high thermal stability.

Supporting Information

Additional TEM images, XPS spectra, Figure S1-S6.

CRediT authorship contribution statement

Chenxiao Wang: Investigation, Formal analysis, Visualization, Writing – original draft. **Ying Lyu:** Investigation, Formal analysis. **Younan Xia:** Conceptualization, Supervision, Funding acquisition, Writing – review & editing, Supervision.

Declaration of Competing Interest

The authors declare that they have no known competing financial interests or personal relationships that could have appeared to influence the work reported in this paper.

Data availability

Data will be made available on request.

Acknowledgements

This work was supported by an NSF grant (CHE-2105602) and startup funds from the Georgia Institute of Technology. The electron microscopy, EDX, and XPS analyses were conducted at the Georgia Tech Institute for Electronics and Nanotechnology, a member of the National Nanotechnology Coordinated Infrastructure (NNCI), which is supported by the National Science Foundation (ECCS-2025462).

Supplementary materials

Supplementary material associated with this article can be found, in the online version, at doi:10.1016/j.susc.2023.122339.

References

- [1] K. Liu, A.Q. Wang, T. Zhang, Recent advances in preferential oxidation of CO reaction over platinum group metal catalysts, ACS Catalysis 2 (6) (2012) 1165–1178
- [2] V.I. Parvulescu, P. Grange, B. Delmon, Catalytic removal of NO, Catalysis Today 46 (4) (1998) 233–316.
- [3] P. Etayo, A. Vidal-Ferran, Rhodium-catalyzed asymmetric hydrogenation as a valuable synthetic tool for the preparation of chiral drugs, Chem. Soc. Rev. 42 (2) (2013) 728–754.
- [4] I. Yakoumis, M. Panou, A.M. Moschovi, D. Panias, Recovery of platinum group metals from spent automotive catalysts: a review, Clean. Eng. Technol. 3 (2021), 100112.
- [5] C.B. Ojeda, F.S. Rojas, Determination of rhodium: since the origins until today ICP-OES and ICP-MS, Talanta 71 (1) (2007) 1–12.
- [6] H. Zhang, W. Li, M. Jin, J. Zeng, T. Yu, D. Yang, Y. Xia, Controlling the morphology of rhodium nanocrystals by manipulating the growth kinetics with a syringe pump, Nano Lett. 11 (2) (2011) 898–903.
- [7] M. Zhao, Z. Chen, Y. Shi, Z.D. Hood, Z. Lyu, M. Xie, M. Chi, Y.A. Xia, Kinetically controlled synthesis of rhodium nanocrystals with different shapes and a comparison study of their thermal and catalytic properties, J. Am. Chem. Soc. 143 (1) (2021) 6293–6302.
- [8] S.R. Lee, M. Vara, Z.D. Hood, M. Zhao, K.D. Gilroy, M. Chi, Y. Xia, Rhodium decahedral nanocrystals: facile synthesis, mechanistic insights, and experimental controls, ChemNanoMat 4 (1) (2018) 66–70.
- [9] S.I. Choi, S.R. Lee, C. Ma, B. Oliy, M. Luo, M. Chi, Y.A. Xia, Facile synthesis of rhodium icosahedra with controlled sizes up to 12 nm, ChemNanoMat 2 (1) (2016) 61–66.
- [10] K. Jang, H.J. Kim, S.U. Son, Low-temperature synthesis of ultrathin rhodium nanoplates via molecular orbital symmetry interaction between rhodium precursors, Chem. Mater. 22 (4) (2010) 1273–1275.
- [11] S. Xie, N. Lu, Z. Xie, J. Wang, M.J. Kim, Y. Xia, Synthesis of Pd–Rh core–frame concave nanocubes and their conversion to rh cubic nanoframes by selective etching of the Pd cores, Angew. Chem. Int. Ed. 51 (41) (2012) 10266–10270.
- [12] S.I. Choi, A. Young, S.R. Lee, C. Ma, M. Luo, M. Chi, C.K. Tsung, Y. Xia, Pd@Rh core-shell nanocrystals with well-defined facets and their enhanced catalytic performance towards CO oxidation, Nanoscale Horiz, 4 (5) (2019) 1232–1238.
- [13] M. Zhao, X. Wang, X. Yang, K.D. Gilroy, D. Qin, Y. Xia, Hollow metal nanocrystals with ultrathin, porous walls and well-controlled surface structures, Adv. Mater. 30 (2018)
- [14] L. Zhang, L.T. Roling, X. Wang, M. Vara, M. Chi, J. Liu, S.I. Choi, J. Park, J. A. Herron, Z. Xie, M. Mavrikakis, Y. Xia, Platinum-based nanocages with subnanometer-thick walls and well-defined, controllable facets, Science 349 (2015) 412–416
- [15] J. Zhu, Z. Chen, M. Xie, Z. Lyu, M. Chi, M. Mavrikakis, W. Jin, Y. Xia, Iridium-based cubic nanocages with 1.1-nm-thick walls: a highly efficient and durable electrocatalyst for water oxidation in an acidic medium, Angew. Chem. Int. Ed. 58 (22) (2019) 7244–7248.

- [16] M. Zhao, L. Xu, M. Vara, A.O. Elnabawy, K.D. Gilroy, Z.D. Hood, S. Zhou, L. Figueroa-Cosme, M.F. Chi, M. Mavrikakis, Y. Xia, Synthesis of Ru icosahedral nanocages with a face-centered-cubic structure and evaluation of their catalytic properties, ACS Catal. 8 (8) (2018) 6948–6960.
- [17] X. Xia, S. Xie, M. Liu, H.C. Peng, N. Lu, J. Wang, M.J. Kim, Y. Xia, On the role of surface diffusion in determining the shape or morphology of noble-metal nanocrystals, Proc. Natl. Acad. Sci. USA 110 (17) (2013) 6669–6673.
- [18] G. Milazzo, S. Carioli, Tables of Standard Electrode Potentials, Wiley, New York, 1979.
- [19] S. Yao, Y. Yuan, C. Xiao, W. Li, Y. Kou, P.J. Dyson, N. Yan, H. Asakura, K. Teramura, T. Tanaka, Insights into the formation mechanism of rhodium nanocubes, J. Phys. Chem. C 116 (28) (2012) 15076–16086.
- [20] M. Jin, H. Liu, H. Zhang, Z. Xie, J. Liu, Y. Xia, Synthesis of Pd nanocrystals enclosed by {100} facets and with sizes < 10 nm for application in CO oxidation, Nano Res. 4 (1) (2011) 83–91.
- [21] B.A.F. Previdello, E. Sibert, M. Maret, Y. Soldo-Olivier, Palladium electrodeposition onto Pt(100): two-layer underpotential deposition, Langmuir 33 (9) (2017) 2087–2095.
- [22] S.N. Tripathi, S.R. Bharadwaj, The Pd-Rh (Palladium-Rhodium) system, J. Phase Equilibria 15 (2) (1994) 208–212.
- [23] T.H. Yang, Y. Shi, A. Janssen, Y. Xia, Surface capping agents and their roles in shape-controlled synthesis of colloidal metal nanocrystals, Angew. Chem. Int. Ed. 59 (36) (2020) 15378–15401.
- [24] S. Xie, H.C. Peng, N. Lu, J. Wang, M.J. Kim, Z. Xie, Y. Xia, Confining the nucleation and overgrowth of Rh to the {111} facets of Pd nanocrystal seeds: the roles of capping agent and surface diffusion, J. Am. Chem. Soc. 135 (44) (2013) 16659, 16667.